Processes controlling extratropical near-tropopause humidity and temperature in the ECMWF global weather forecast model

Received: 11 April 2024 | Revised: 6 September 2024 | Accepted: 17 September 2024

DOI: 10.1002/qj.4873

Quarterly Journal of the Royal Meteorological Society RMetS

RESEARCH ARTICLE

Processes controlling extratropical near-tropopause humidity and temperature in the ECMWF global weather forecast model

Jake Bland[1] | **Richard Forbes**[2] | **Suzanne L. Gray**[1] | **John Methven**[1]

[1]Department of Meteorology, University of Reading, UK

[2]ECMWF, Reading, UK

Correspondence
Jake Bland, Department of Meteorology, University of Reading, UK.
Email: jake.bland@reading.ac.uk

Funding information
Natural Environment Research Council, Grant/Award Number: NE/L002566/1

Abstract

Accurate representation of near-tropopause fields is important for the forecast skill of numerical weather prediction models, yet there remain significant systematic forecast errors in the region of the tropopause. Although extratropical near-tropopause humidity, temperature, and wind model biases have been documented from several models, more knowledge of their causes is required as a step towards reducing these biases. Typically, a moist bias is present in the lowermost stratosphere in the analyses used to initialise forecasts, which leads to a growing cold bias in the lowermost stratosphere over the course of the forecasts due to long-wave radiative cooling. Experiments are conducted with the European Centre of Medium-Range Weather Forecasts global forecast system where the humidity in a layer 0–4 km above the tropopause in the extratropics is reduced to correct the moist bias in the initial conditions. In these experiments, the lowermost stratosphere cold bias growth is halved compared with the control and gradually remoistens, returning to typical analysis values with a half-life of around 8–9 days. The reduction in cooling in the lowermost stratosphere is due to a reduction in long-wave radiative emission from the water vapour above the tropopause. The main contributors to the remoistening are resolved advective transport and parametrised turbulent mixing in the model, the cloud microphysical process rates being similar in the modified and control experiments. The biases in near-tropopause moisture transport are almost independent of horizontal resolution. These results show that the temperature bias in the extratropical lower stratosphere can be reduced by correcting the collocated moist bias, but the moist bias cannot be fixed by solely correcting the initial conditions and further model improvements are also required to reduce cross-tropopause moisture transport.

KEYWORDS

atmosphere, extratropical weather systems, humidity, midlatitude, numerical methods and NWP, radiation, stratosphere, tropopause

1 | INTRODUCTION

There is a cold bias in the lowermost stratosphere of many weather forecast and climate models (Lawrence *et al.*, 2022; Shepherd *et al.*, 2018; Wu & Reichler, 2020), and it has further been shown that there is a coincident moist bias present in analyses, reanalyses, and forecasts (Dyroff *et al.*, 2015; Kunz *et al.*, 2014; Oikonomou & O'Neill, 2006; Woiwode *et al.*, 2020). Results from single column modelling with the European Centre of Medium-Range Weather Forecasts (ECMWF) model (Bland *et al.*, 2021) indicate that the cooling of the forecasts with respect to the analysis is consistent with the additional long-wave radiative cooling expected from the excessive water vapour in the lowermost stratosphere of the model. In this article we refer to the lowest 2–3 km above the tropopause as the lowermost stratosphere, in the extratropics. Across this region, thermodynamic and chemical properties transition from those typical of the troposphere to those typical of the stratosphere.

The impacts of cooling and/or moistening at the tropopause level on global circulation have been investigated in global models either through the increase of stratospheric water vapour (Joshi *et al.*, 2006; Maycock *et al.*, 2013) or direct imposition of stratospheric or tropopause-level cooling (Boljka & Birner, 2022; Tandon *et al.*, 2011). It has been shown that such biases result in a strengthened and poleward-shifted subtropical jet, in addition to an influence on the strength and width of the Hadley circulation: Tandon *et al.* (2011) imposed cooling to mimic an increase in water vapour and found a weakened Hadley cell; however, Boljka and Birner (2022) used cooling to strengthen the tropopause inversion layer and instead found a strengthened Hadley cell. Wu and Reichler (2020) suggest the cold bias impacts not only the accurate forecasting of stratospheric events such as sudden stratospheric warmings but also weather in the troposphere.

A key unanswered problem, which is the focus of this study, is the cause of the moist bias in the lowermost stratosphere in model analyses and forecasts and how this can be corrected. Cloud processes can influence stratospheric water vapour in the Subtropics and midlatitudes. Deep convection overshooting the tropopause can transport water to the lower stratosphere, where it can evaporate or sublimate and increase local humidity, as has been identified in studies such as Jensen *et al.* (2020) over North America. Furthermore, Müller *et al.* (2015) find evidence of ice crystals from cirrus clouds formed in the troposphere being transported into the extratropical lowermost stratosphere, which can then sublimate to provide an additional source for moistening in the lowermost stratosphere.

Another important factor controlling moisture in the stratosphere is transport from the Tropics (Bönisch *et al.*, 2009; Gettelman *et al.*, 2010). As a part of the Brewer–Dobson circulation, there is large-scale ascent in the Tropics. There are then two pathways by which air is transported to the extratropical stratosphere: entering the tropical lower stratosphere via upward transport through the tropical tropopause, and moving up towards the stratopause as it moves polewards before descending at midlatitudes, or moving polewards isentropically entering the stratosphere in the Subtropics. The coldest part of the troposphere is in the Tropics, and air transported through this region will be dried due to condensation or ice deposition, reducing the vapour pressure to the low saturation vapour pressure associated with such cold temperatures. Tropospheric air can also be mixed into the extratropical lowermost stratosphere as a result of mixing processes such as Kelvin–Helmholtz instability across the tropopause (Kunkel *et al.*, 2019), or the creation of filaments of tropospheric air by Rossby-wave breaking events, which are then stretched to increasingly fine scales (Bradshaw *et al.*, 2002; O'Connor *et al.*, 1999; Vaughan & Timmis, 1998). It has been identified by Hardiman *et al.* (2015) that, in the Met Office Unified Model, a warm tropical tropopause layer is at least somewhat responsible for a moist bias of the tropical lower stratosphere, as a warmer tropical tropopause layer has a higher saturation vapour pressure, and hence more water vapour can be transported across the tropopause. The Integrated Forecasting System (IFS), however, has a cold bias at the tropical tropopause (Polichtchouk *et al.*, 2019b); so, although poleward transport is still an important factor when considering water vapour in the extratropical lowermost stratosphere, the moist bias cannot necessarily be explained in the same way across all models. Another process that is a source of water vapour in the stratosphere is the oxidation of methane that occurs in the upper branch of the Brewer–Dobson circulation; however, this process is more relevant to the upper stratosphere and has little impact in the extratropical lowermost stratosphere (Noël *et al.*, 2018).

It was established by Bland *et al.* (2021; hereafter referred to as B21) that the moist bias present in the initial conditions for operational ECMWF IFS and Met Office Unified Model forecasts changes very little during a 5-day forecast. Noted also in B21 are the difficulties associated with the assimilation of humidity observations in the stratosphere. Humidity increments are not applied above the tropopause during data assimilation in the IFS (Ingleby, 2017). With no contribution from observations we hypothesise that the moist-biased analysis state is a consequence of a bias in the representation of model processes. To investigate this bias in the present study, IFS

reforecasts are run with a correction applied to the initial humidity field to bring this as close as possible to the available observations. The sensitivity to the initial humidity in the lowermost stratosphere is then used to infer possible factors contributing to the IFS humidity and temperature biases.

Following from this, the aims of this study are as follows:

1. Determine the evolution of the vertical structure of moisture in the upper troposphere and lower stratosphere (UTLS) region as the moisture bias in the lowermost stratosphere re-establishes itself after correction.
2. Determine the vertical structure and generation time-scale of the temperature bias in the UTLS region due to the model bias in moisture in the lowermost stratosphere in the analysis, and the associated impact on tropopause altitude.
3. Attribute the moisture and temperature biases in the UTLS region to model processes.
4. Determine the sensitivity of the results to model horizontal resolution.

In Section 2 we provide information on the model and data used to carry out this study. The methods used to address our aims are outlined in Section 3, before describing the impacts of the initial humidity reduction on humidity and temperature in the forecasts in Section 4. In Section 5 we initially determine the physical parametrisations that dominate the evolution of UTLS temperature, and subsequently discuss what the process tendencies tell us about the model treatment of water vapour. Section 6 expands upon this by also considering such tendencies in forecasts run at different horizontal resolutions. Finally, a discussion and conclusions are provided in Section 7.

2 | MODEL AND OBSERVATIONAL DATA

To address the aims presented in Section 1, we use data from forecasts that were performed with the ECMWF IFS cycle 47R1 (ECMWF, 2020), which was operational between June 2020 and May 2021. One of the major improvements of 47R1 over previous model versions is the introduction of the higher order quintic vertical interpolation instead of cubic for water vapour (Polichtchouk *et al.*, 2020). Prior to this, forecasts at higher horizontal resolutions would generate waves at too small a scale to be resolved in the vertical, leading to unphysical grid-scale oscillations in the vertical that caused excessive cooling in the stratosphere. The use of this IFS cycle means that our analysis considers the bias that remains in the lowermost stratosphere after this correction.

Forecasts were run at three different horizontal resolutions: the current resolution for operational medium-range numerical weather prediction at ECMWF with a grid spacing of approximately 9 km (TCo1279), and lower resolutions with grid spacings of approximately 25 km (TCo399) and 50 km (TCo199), covering the range of resolutions used for extended-range and seasonal forecasts at ECMWF. The "TCo" prefix here stands for triangular cubic-octahedral, a detailed explanation of which can be found in Malardel *et al.* (2016). All forecasts have 137 model levels in the vertical, which corresponds to a vertical spacing of around 250 m near the tropopause.

We consider sets of 30 forecasts initialised at 0000 UTC each day from the September 15 to October 14, 2016. This period is chosen to coincide with the North Atlantic Waveguide and Downstream Impact Experiment (NAWDEX) field campaign (Schäfler *et al.*, 2018), from which radiosonde observations were used by B21 to characterise UTLS temperature and humidity biases. Forecasts are run for lengths of both 5 and 15 days. Preliminary year-long experiments run at TCo199 indicated that 15 days is an appropriate time-scale to observe the differences in development of humidity and temperature biases between experiments.

To investigate the processes responsible for changes to the temperature and humidity fields in the lowermost stratosphere in the model, tendencies from the dynamics and physical parametrisations are output from the 5-day forecasts. As an example, Rodwell and Palmer (2007) considered the forecast tendencies in the model that evolve the state prior to the application of the analysis increment in the assimilation cycle in their initial tendency methodology. For the analysis presented in this study we consider process tendencies accumulated over the longer period of 5 days, which allows for the investigation of the time variation of the tendencies as the fields adjust. To look at the characteristics of their evolution, and differences between experiments, the tendencies are archived 12 hourly for TCo199 and TCo399 and 24 hourly for TCo1279.

Observations used to constrain the humidity correction are taken from both radiosondes and the *Aura* microwave limb sounder (MLS). Radiosonde data from the NAWDEX campaign used here are from the European Meteorological Services Network as described in Schäfler *et al.* (2018). The radiosondes types are a mix of Vaisala RS92 (Vaisala, 2013) and RS41 (Vaisala, 2018), and a more in-depth discussion of these can be found in B21. MLS data are obtained from the Goddard Earth Sciences Data and Information Services Center (Lambert *et al.*, 2020) and used only between 40°N and 60°N at pressures below 316 hPa. The satellite data used have been binned daily

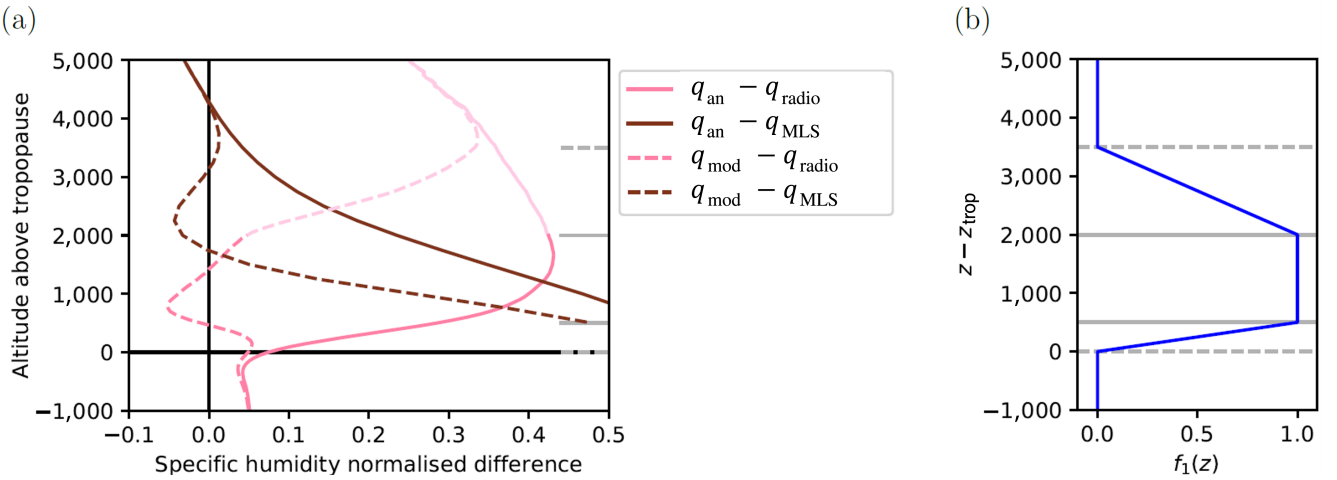

FIGURE 1 (a) Normalised difference in specific humidity comparing the analysis humidity q_{an} (solid) and modified initial conditions from QMOD experiment q_{mod} (dashed) with the radiosonde data q_{radio} (pink curves, or light grey in greyscale) and *Aura* microwave limb sounder (MLS) satellite data q_{MLS} (brown curves, or dark grey in greyscale). It is noted in B21 that the radiosonde observations are less reliable above 2 km above the tropopause, and so the lines are faded above this point to indicate this. The MLS satellite retrievals are less reliable within 1.5 km of the tropopause. (b) Illustration of the vertical structure of $f_1(z)$ with horizontal lines to indicate altitudes defining the humidity modification function. Similar lines are included on the right to panel (a). [Colour figure can be viewed at wileyonlinelibrary.com]

onto a regular grid ("Level 3" data), considering only bins with ≥1 valid data points. MLS observations are compared with IFS analysis fields at 1200 UTC, with the IFS analysis tropopause altitude used for tropopause-relative composition when required, as for Figure 1 in Section 3. Further details for the MLS data can be found in Livesey *et al.* (2020), with information on water vapour retrieval in their section 3.9, and the Level 3 datasets in their section 4.

3 | METHODS

In this section we describe the method used to reduce the humidity in the lowermost stratosphere to realistic values for the experimental forecasts, the use of tropopause-relative coordinates, the Eulerian process tendencies used to attribute changes in temperature and humidity to model parametrisations, and the methods used for compositing and masking of data.

3.1 | Initial humidity reduction

To investigate the effects of the moist bias in the lowermost stratosphere on the model behaviour we run one set of forecasts with the humidity field from the analysis (termed CTRL) and another set of forecasts in which the specific humidity is reduced in the lowermost stratosphere at the start of the forecast, to be in closer agreement with observations at the initial time (termed QMOD). The structure and magnitude of this reduction is based on the tropopause-altitude-relative humidity bias identified in B21 through comparison of operational analyses to radiosonde humidity measurements, shown also in Figure 1a. Note that, for the comparison in the figures, the specific humidity normalised difference (here denoted $\widehat{\Delta q}$) between two humidity profiles q_A and q_B is calculated as in B21:

$$\widehat{\Delta q} \equiv \frac{q_A - q_B}{\sqrt{q_A^2 + q_B^2}}.$$

Given that we do not have detailed knowledge of the humidity bias at every location and time, we approximate the mean bias correction with a simple function of pressure and tropopause-relative altitude. The equation for the reduction of the humidity is applied globally and takes the form

$$q_{mod}(p,z) = q_{an}(p,z) - q_{an}(p,z) \times f(p,z), \qquad (1)$$

where q_{mod} is the modified humidity field that is used to initialise the QMOD forecasts, q_{an} the analysis humidity field, p (Pa) and z (m) the model pressure and altitude respectively, and f the factor by which the humidity is reduced. This factor can be expressed as the product $f(p,z) = f_{max} \times f_1(z) \times f_2(p)$, where $0 < f_{max}, f_1, f_2 < 1$ for all p, z. Here, altitude is used to constrain distance above the tropopause, and pressure is used to smooth the function going towards the Tropics.

The radiosonde observations can be used to define $f_1(z)$ for altitudes $z > z_{trop}$, where z_{trop} is the altitude of

the model tropopause in a column at a given latitude and longitude as calculated using the standard World Meteorological Organization lapse rate definition. We define

$$f_1(z) = \begin{cases} 0 & z < z_{\text{trop}} \\ \frac{z - z_{\text{trop}}}{500} & z_{\text{trop}} < z < z_{\text{trop}} + 500 \\ 1 & z_{\text{trop}} + 500 \le z \le z_{\text{trop}} + 2{,}000 \end{cases}, \quad (2)$$

where z is in units of metres. The linear reduction in the 500 m above the tropopause covers two or three model levels and moderates the sharpness of the gradient we are introducing here. As we have less confidence in the radiosonde observations for $z > z_{\text{trop}} + 2{,}000$ m, we consider also a comparison of the model analysis humidity field to observations from the *Aura* MLS satellite instrument (Lambert *et al.*, 2020). Despite the coarser resolution of these observations in the vertical compared to the radiosonde observations, the MLS observations show that the moist bias in analyses is largely confined to the lowermost stratosphere within 3.5 km of the tropopause (brown solid line in Figure 1a). Humidity reduction factors that dry the atmosphere at higher levels were shown to worsen the agreement with these MLS observations. Note however that the MLS data are less reliable in the lowest 1.5 km above the tropopause (because the accuracy becomes worse as pressure increases from 30 hPa towards 300 hPa (Livesey *et al.*, 2020)) so we trust the radiosonde data there.

To avoid the introduction of a sharp humidity gradient at the top of our dried layer the modification function declines linearly with height:

$$f_1(z) = \begin{cases} \frac{3{,}500 + z_{\text{trop}} - z}{1{,}500} & z_{\text{trop}} + 2{,}000 \le z \\ & \quad \le z_{\text{trop}} + 3{,}500. \\ 0 & z > z_{\text{trop}} + 3{,}500 \end{cases} \quad (3)$$

The function $f_1(z)$ is illustrated in Figure 1b. Furthermore, the model moist bias that we are investigating is confined to the extratropics. To prevent humidity reduction in the Tropics, while also avoiding the introduction of an unphysical sharp meridional humidity gradient, instead of making q_{mod} a function of latitude we take advantage of the fact that the pressure at the tropopause generally decreases towards the equator, and we do not have evidence of a moist bias at lower pressures higher in the stratosphere. Therefore we have

$$f_2(p) = \begin{cases} 0 & p < 10{,}000 \\ \frac{p - 10{,}000}{5{,}000} & 10{,}000 \le p \le 15{,}000, \\ 1 & p > 15{,}000 \end{cases} \quad (4)$$

where p is in units of pascals. Finally, we use a maximum reduction factor $f_{\max} = 0.55$. The reduction factor obtained through the product of the combination of the aforementioned choices of $f_{\max}, f_1$, and f_2 gives the greatest agreement with the available observations in magnitude and mean structure that we can achieve while keeping the method relatively simple.

Figure 1a illustrates that the normalised difference between the adjusted initial conditions, q_{mod}, and the radiosonde observations is near zero on average between the tropopause and 2 km above (pink dashed curve). Above this level (where radiosonde humidity measurements are uncertain), the normalised difference between q_{mod} and the MLS observations is near zero (brown dashed curve). Therefore, it can be concluded that the modified field q_{mod} is a better representation of the atmospheric state and closer to the best observational measurements at each level than the operational analysis.

By making the adjustment in a tropopause-relative sense we assume that the correction will be appropriate for every profile. However, it was noted in B21 that the vertical tropopause-relative structure of the moist bias differs from the mean in tropopause trough regions. Such differences for regions of low tropopause altitude have also been observed by Krüger *et al.* (2022). A humidity modification function $f_1(z, z_{\text{trop}})$ that varied not only with altitude within a given profile but also according to tropopause altitude, yielding a different structure when the tropopause altitude was low, was also trialled (not shown) but performed so similarly to the simpler formula presented herein that the additional complexity was not justified.

3.2 | Tropopause-relative coordinates

We are considering fields in close proximity to the tropopause, with particular interest in the dependence of the values of these fields on their vertical position relative to the tropopause. We want to visualise these fields and take composites in a tropopause-relative framework. However, issues arise as a result of the tropopause being an interface associated with sharp gradients, and hence markedly different properties on either side, which varies in time, space, and also between profiles at the same spatial and temporal location in differing datasets.

We regrid fields to an altitude coordinate relative to a tropopause altitude that is the same, at a given latitude, longitude, and time, between all data sources in any given comparison. This regridding is so we can compare like-for-like regions of the atmosphere on a profile-by-profile basis in a way that is not sensitive to the particular thresholds chosen for the definition of

the tropopause. The method used is to regrid fields in the vertical from model level coordinates (of the 137 model levels) to $\overline{z} - \overline{z}_{\text{trop}}$ coordinates, where z are the altitudes of the model levels considered, z_{trop} is the altitude of the tropopause, and the overbar refers to the arithmetic mean between the values in the two datasets being compared, which is typically a model forecast and analysis. It is necessary to take the mean between the tropopause altitudes from the two datasets as comparing fields from two datasets relative to the tropopause determined from just one of these datasets can lead to sizeable systematic errors in composites. This error occurs even if there are no systematic differences in the altitude or tropopause altitude between the two datasets. This is due to the changes in vertical gradients of the fields of interest across the tropopause, meaning vertical displacements of profiles of equal magnitudes but opposite directions lead to differences of unequal magnitudes, which when averaged yield non-zero results (not shown).

3.3 | Cumulative tendency budget

To determine the model processes responsible for changes to the fields of temperature and humidity over the course of the forecast, the time-step tendencies from each component of the model—that is, from individual physical parametrisations and the dynamics—are accumulated at each grid point through the forecast. Hence, these are the cumulative Eulerian process tendencies that, when added together, equal the total tendency for the time period. For better visualisation in a tropopause-relative sense, these whole forecast cumulative tendencies are decomposed into 12-hourly cumulative tendencies such that

$$x^{\text{tend}}_{12\text{ hrly}}(t) = x^{\text{tend}}_{\text{cumul.}}(t) - x^{\text{tend}}_{\text{cumul.}}(t-12), \tag{5}$$

where t is time in hours, and $x^{\text{tend}}_{\text{cumul.}}$ and $x^{\text{tend}}_{12\text{ hrly}}$ are, respectively, the whole forecast cumulative (from times zero to t) and 12-hourly cumulative (from times $t-12$ to t) tendencies of the variable x (either temperature or specific humidity) due to some process tend. Consequently, as $x^{\text{tend}}_{12\text{ hrly}}(t)$ is the change resulting from the process tend centred on time $t-6$, it does not make sense to use $(\overline{z}(t) - \overline{z}_{\text{trop}}(t))$ as our tropopause-relative altitude coordinate as defined in the previous subsection. Therefore, we instead use

$$\frac{(\overline{z}(t) - \overline{z}_{\text{trop}}(t)) + (\overline{z}(t-12) - \overline{z}_{\text{trop}}(t-12))}{2} \approx (\overline{z}(t-6) - \overline{z}_{\text{trop}}(t-6)). \tag{6}$$

Additionally, the specific humidity 12-hourly cumulative tendencies will be primarily expressed as a fraction of the mean humidity background state in the centre of this window, $q^{\text{tend}}_{12\text{ hrly}}(t)/\overline{q}(t-6)$, where $\overline{q}(t-6)$ is the arithmetic mean of $\overline{q}(t)$ and $\overline{q}(t-12)$ as for z earlier.

3.4 | Compositing and masking

In addition to the processing already described, data are also masked for regions where $\overline{z} < 0$ before compositing. For composites, a latitude-weighted arithmetic mean is taken over fields and differences between fields over the latitude band 40–75°N, and then a further mean is taken over data from each date and time at which a forecast was initialised.

4 | CONTROL OF HUMIDITY IN THE LOWERMOST STRATOSPHERE ON THE STATE OF THE UTLS IN 15-DAY FORECASTS

In this section we outline the main differences in specific humidity, temperature, and tropopause altitude between the set of QMOD forecasts that have the humidity initial bias correction in the lowermost stratosphere, the set of control (CTRL) forecasts, and the unmodified control analysis. Three different resolutions are considered.

4.1 | Differences in humidity

We first consider the humidity field, as it is differences in the humidity that we anticipate will force the behaviour of other model variables. Figure 2a shows the mean difference between specific humidity in the midlatitude Northern Hemisphere in forecasts and the analysis as a function of altitude relative to the tropopause height using the method detailed in Section 3. The difference for QMOD at day 1 is very similar to the difference that we impose in the lowermost stratosphere (as expected, given that the difference has not had much time to change), and is therefore the same at all three horizontal resolutions considered, although only the mid-resolution results are shown in Figure 2a.

Looking at the evolution of the mean difference in humidity after 5 and 15 days into the forecast, the difference between the QMOD forecast and unmodified analysis humidity in the lowermost stratosphere decreases with increasing forecast lead time (i.e., there is a

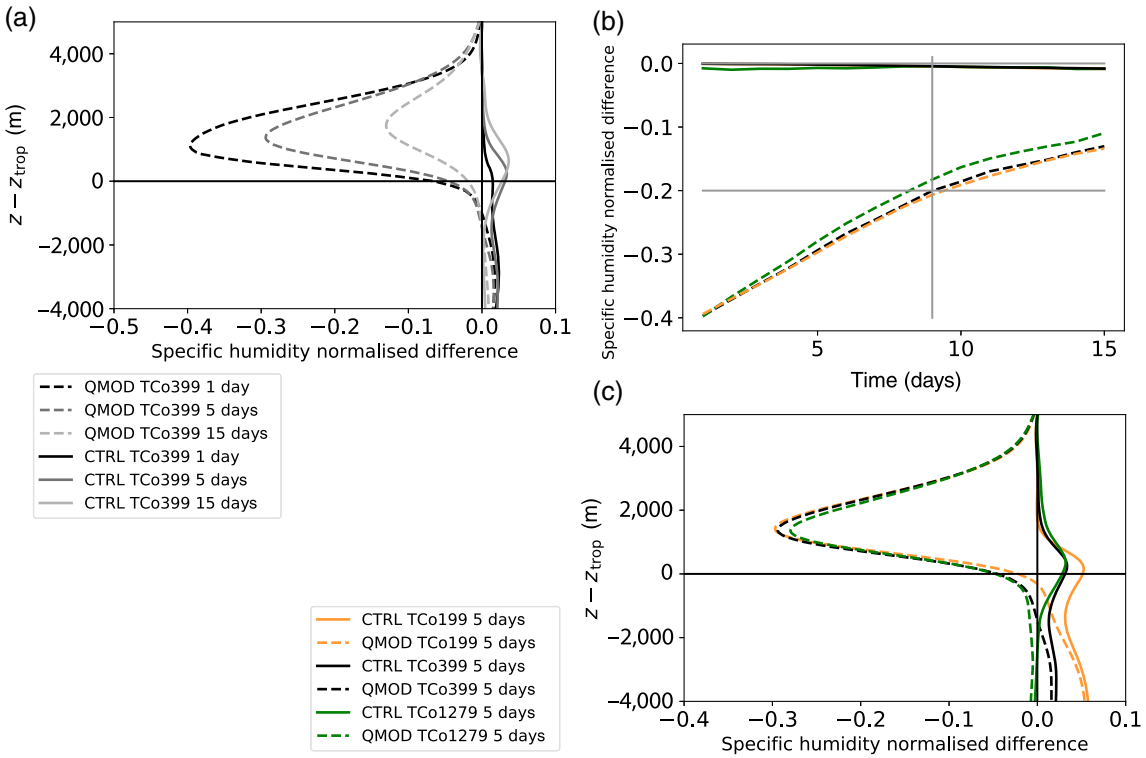

FIGURE 2 (a) Tropopause-relative vertical profiles of specific humidity normalised difference between forecast experiments (resolution TCo399) and analysis at lead times of 1 day (black), 5 days (grey), and 15 days (light grey) into the forecast, with CTRL in solid lines and QMOD dashed. (b) The minimum normalised difference in 12-hourly mean vertical profiles as a function of lead time, showing experiments with resolution TCo199 (orange or light grey in greyscale), 399 (black), and 1,279 (green or dark grey in greyscale). Additional grey lines mark a normalised difference of −0.2, and day 9. (c) Vertical profiles, as in (a), at 5-day lead time for each of these three horizontal resolutions. [Colour figure can be viewed at wileyonlinelibrary.com]

remoistening above the tropopause), whereas the humidity in the CTRL forecasts remains fairly similar to the analysis, suggesting there is a preferred equilibrium of humidity in the model. It can be seen from Figure 2b that the initial humidity difference halves within the first 8–9 days. Starting at a mean normalised difference of −0.4, this corresponds to an increase of around 2.5% (of the background value) per day. As the QMOD humidity field becomes closer to the analysis, the rate at which the difference decreases slows.

The specific humidity remoistening in the lowermost stratosphere is very similar between the three resolutions investigated, as can be seen from Figure 2c. In the lowermost stratosphere, QMOD forecasts for the highest resolution of TCo1279 are slightly closer to the analysis after 5 days (i.e., the peak negative normalised difference has the smallest magnitude). However, at the altitude of this peak difference (at about 1.5 km), the corresponding CTRL forecasts are furthest from the analysis (in the opposite direction), so the differences between the QMOD and CTRL forecasts are similar for all three resolutions.

To gain further insights into the differences in the rate of relative remoistening as a function of both altitude and latitude, we consider Figure 3. The quantity presented here is one minus the fraction of the total imposed drying that remains after 5 and 15 days. More precisely, it is calculated as $1 - (\widehat{\Delta q}(t)/\widehat{\Delta q}(1))$, with the normalised difference being between QMOD and the analysis, and time $t = 1$ the earliest time available in the forecast after the humidity modification has been applied. Therefore, a value of zero in Figure 3 indicates that no additional moisture has been introduced to the region between times 1 and t, and a value of 1 indicates that humidity values have returned to be the same as the analysis. Within the first 5 days of the forecast we note both that the remoistening is largest closest to the tropopause and that it is of a very similar magnitude across latitudes, though being slightly larger in the 40–50°N range closest to the Subtropics. A much larger latitude dependence can be noted, however, considering forecasts out to 15 days, with the specific humidity in the lowermost stratosphere being increased towards the analysis values around twice as much at 40–50°N compared with at 70–80°N.

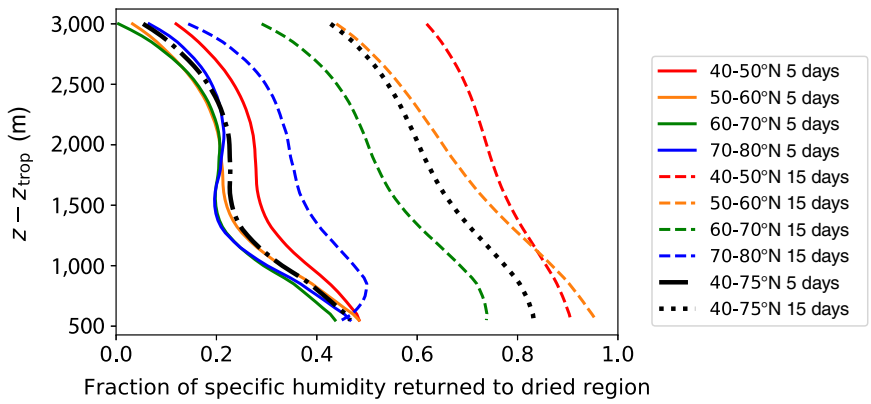

FIGURE 3 Fraction of the specific humidity removed from the lowermost stratosphere that has been reintroduced by model processes (see equation in accompanying text) after 5 and 15 days of the forecast, as a function of latitude. Area-weighted means are taken over latitude bands of 10°. Black lines indicate means over the 40–75°N range as for all other figures in this article. Solid and dot-dash lines are for 5-day and dashed and dotted lines for 15-day forecasts. [Colour figure can be viewed at wileyonlinelibrary.com]

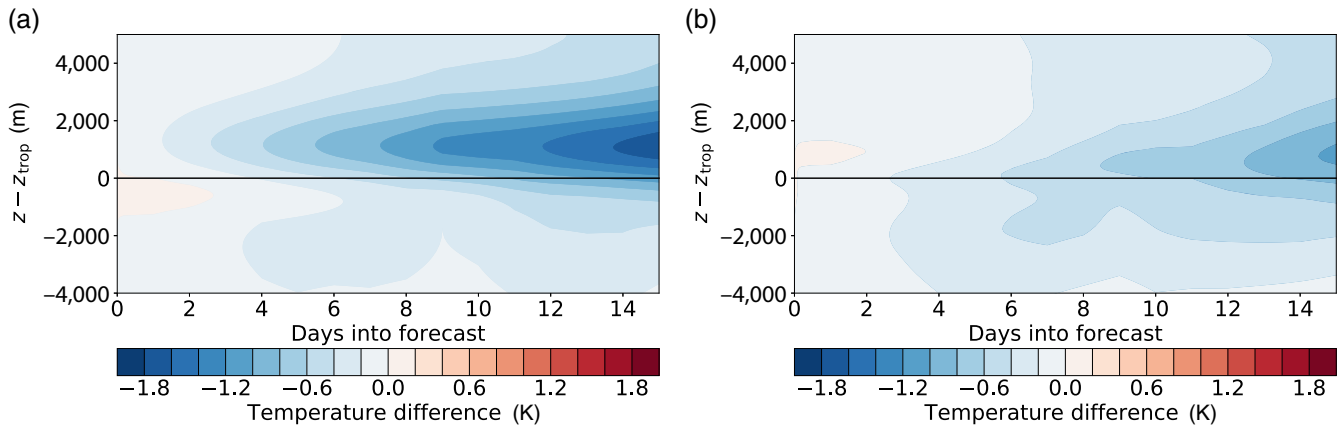

FIGURE 4 Time series of the mean difference in temperature for experiments (a) CTRL and (b) QMOD (at resolution TCo399) relative to the operational analysis. [Colour figure can be viewed at wileyonlinelibrary.com]

4.2 | Impacts on temperature and tropopause altitude

We now look at the response of temperature and tropopause altitude to the removal of moisture in the lowermost stratosphere. The development of an extratropical cold bias in the lowermost stratosphere in forecasts is well known, and evidence is discussed in Section 1. This cold bias development in forecasts is illustrated in Figure 4a for the midresolution forecasts, with the temperature in the CTRL forecast becoming colder than that in the analysis by around $-0.15\,\mathrm{K\cdot day^{-1}}$ at the altitude where the magnitude of the difference peaks. From the single column experiments of B21 it was concluded that this rate of cold bias growth was consistent with, if slightly in excess of, that which would be expected to result solely from additional long-wave cooling in the presence of the positive moist bias in the lowermost stratosphere.

Figure 4b shows the evolution of the difference between the QMOD forecast and analysis temperature in the 15-day forecasts. In this panel the temperature bias develops at an approximately halved rate of around $0.07\,\mathrm{K\cdot day^{-1}}$. The difference in cooling between CTRL and QMOD is shown again in Figure 5a for snapshots at 1, 5, and 15 days into the forecasts, and the approximately constant respective peak cooling rates throughout the forecasts are shown in Figure 5b. Similar to the humidity in Figure 2b, the rate of change of the cooling difference begins to slow slightly after about day 9, and is particularly evident in the CTRL forecasts. If Figure 5a is split according to latitude band as for Figure 3 (not shown) we additionally find that the cold bias is largest between 50°N and 60°N, becoming smaller both polewards and equatorwards of this and vanishing south of 40°N. A similar meridional location of the peak magnitude of the cold bias can also be seen in the zonally averaged cross-sections of, for example, Polichtchouk *et al.* (2019a) or Charlesworth *et al.* (2023).

In CTRL, with the specific humidity field in its biased quasi-equilibrium state, the temperature tends towards an equilibrium with this humidity field in the forecast,

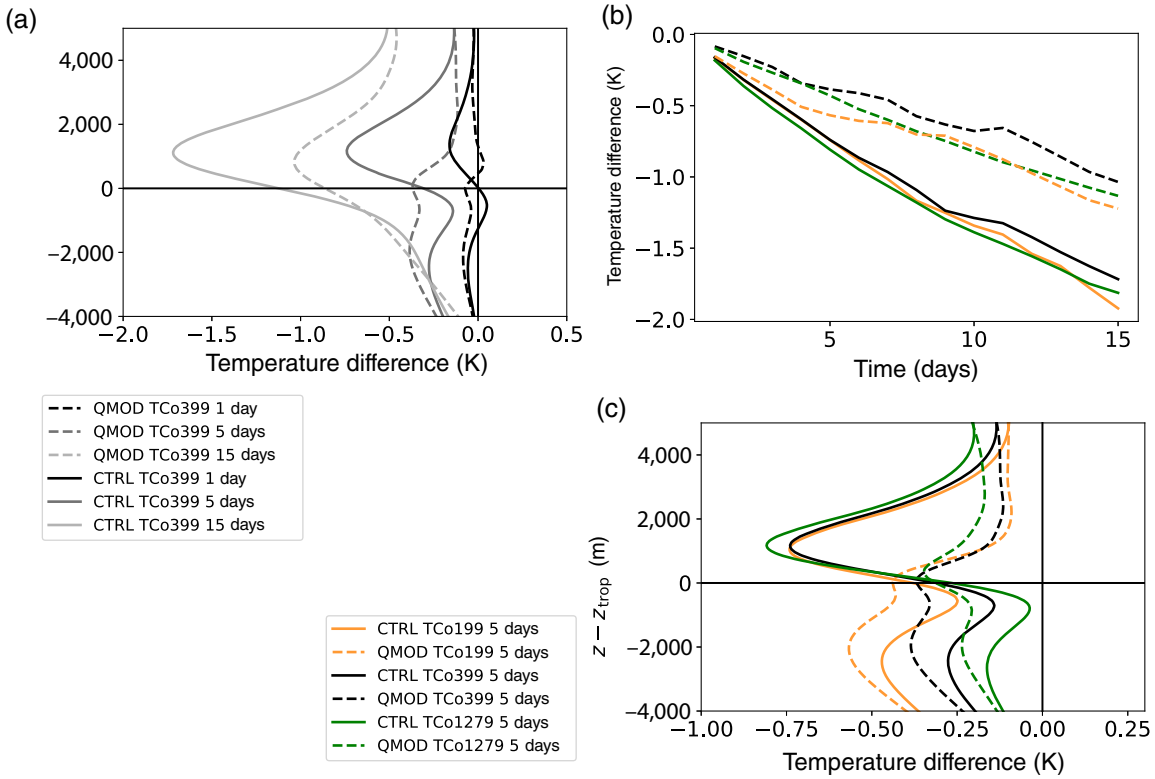

FIGURE 5 As for Figure 2, but showing the temperature difference from operational analyses instead of specific humidity difference. [Colour figure can be viewed at wileyonlinelibrary.com]

which is corrected in each operational analysis cycle by temperature increments during the data assimilation. However, in QMOD, even though the humidity bias is corrected, there is still a growth of a cold bias, albeit at a reduced rate. This could be because of the gradual reintroduction of moisture into the lowermost stratosphere (Figure 2b), although this would take time to build up and affect the temperature. It could also be because the humidity correction, although in agreement with observations in a mean sense, is not correcting the humidity with quite the right spatial and temporal structure, or there could be other reasons for the growth of the remaining cold bias.

From the idealised experiments of B21 (their Section 5), the expected radiative response of the near-tropopause temperature to an overabundance of water vapour in the lowermost stratosphere is one of both excessive cooling in the lower stratosphere and of warming in the upper troposphere. However, such a tropospheric warming bias in the forecasts was not present in the comparisons of operational forecasts with the radiosonde observations in B21. Here, too, in the upper troposphere, the CTRL forecasts are not systematically warmer than the analysis. Now looking at the impact of the moist bias in the lowermost stratosphere by comparing CTRL with QMOD (solid lines with the dashed lines in Figure 5a,c), not only is there the expected relative cooling in the lowermost stratosphere from the moist bias, but there is also additional warming in the upper troposphere in CTRL. This is consistent with what we would expect from the introduction of a moist layer above the upper tropopause (Cau *et al.*, 2005). However, the difference between the upper troposphere temperature in CTRL and QMOD is less than that in the lowermost stratosphere, as we expect the shorter mixing time-scales of the troposphere to more rapidly dissipate any radiatively induced temperature differences.

The resolution dependence of the temperature bias is shown in Figure 5b,c. Similar to the specific humidity profiles, there is very little difference in temperature bias development in the lowermost stratosphere with respect to the analysis between varying horizontal resolutions. However, there is a notable difference between the three model resolutions in the troposphere (Figure 5c), with colder temperatures at lower resolutions. A similar difference can be seen in Figure 2c, with slightly moister profiles at lower resolutions at day 5. This is likely due to a different balance of dynamical and physical processes in the troposphere at lower resolutions, leading to a different equilibrium state compared with the TCo1279 analysis from which the lower resolution simulations are also initialised and compared with. This resolution difference in the troposphere is not connected to the imposed moisture

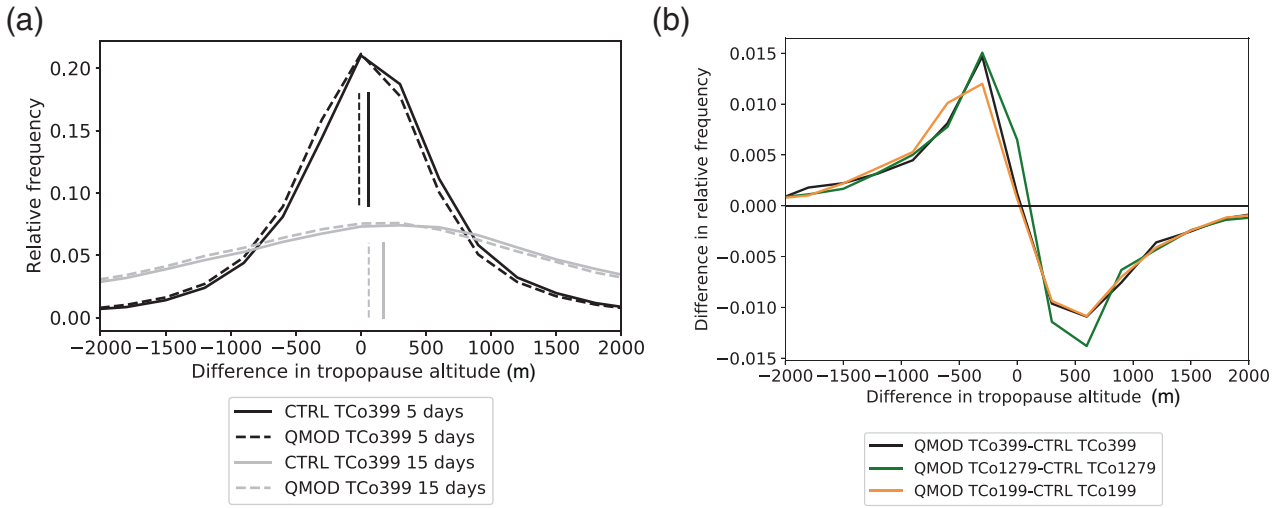

FIGURE 6 (a) Relative frequencies of difference in tropopause altitude between TCo399 forecast and analysis using 300 m bins 5 days (black) and 15 days (grey) into the forecast for both CTRL (solid) and QMOD (dashed). Vertical lines indicate the means for each distribution. (b) QMOD minus CTRL differences in the relative frequencies as in (a) at day 5 for TCo199 (orange or light grey in greyscale), 399 (black), and 1279 (green or dark grey in greyscale). [Colour figure can be viewed at wileyonlinelibrary.com]

difference, and therefore not relevant to the aims of this study.

We are defining the tropopause based on the temperature lapse rate; therefore, systematic changes in temperature will also be expected to result in systematic changes in the identified tropopause altitude. B21 explained how the structure of the temperature bias resulting from the moist bias in the lowermost stratosphere would lead to a systematic positive bias in the tropopause altitude in forecasts. Figure 6a illustrates how the reduction of humidity in the lowermost stratosphere in QMOD shifts the distribution of the tropopause altitude difference from the analysis towards lower values compared with the CTRL. In the CTRL forecasts the tropopause is systematically at a slightly higher altitude than the analysis, increasing with lead time, whereas this bias is reduced for QMOD. The difference between the 5-day QMOD and CTRL frequency distributions for TCo399 from Figure 6a are shown in Figure 6b along with those from TCo199 and TCo1279, further highlighting the tropopause shift and indicating that it, too, is largely independent of horizontal resolution.

5 | MODEL PROCESSES CONTROLLING THE DIFFERENCES IN FORECAST EVOLUTION OVER THE FIRST 5 DAYS

In this section we make use of the partition of the changes to the prognostic model fields into Eulerian tendencies as introduced in Section 3.3. As the addition of many three-dimensional fields to the model is very expensive, tendencies have only been implemented in shorter 5-day forecasts. Considering these tendencies, we investigate both the factors influencing UTLS temperature, which lead to the development of the forecast cold bias in the lowermost stratosphere, and those controlling water vapour, to elucidate mechanisms that are most likely to contribute to the presence of the model moist bias in the extratropical lowermost stratosphere. The physical processes affecting both temperature and specific humidity shown in the following subsections are subgrid turbulent mixing in the vertical ("vertical diffusion"), cloud processes (primarily ice deposition at UTLS temperatures), and convection. Also shown are the cumulative changes to the temperature and humidity fields following the solution of the model dynamics in each time step. For temperature, we additionally consider the effects of long-wave and short-wave radiation and gravity wave drag.

5.1 | Processes controlling temperature

Before examining the ways in which the influence of the process tendencies on temperature differs between the CTRL and QMOD forecasts, first consider Figure 7a, which illustrates the mean 12-hourly impact of each of the processes on temperature in a tropopause-relative frame of reference. For the CTRL forecast we can see the long-wave cooling throughout the depth of the UTLS (which is stronger in the moister upper troposphere), warming through the absorption of short-wave radiation following

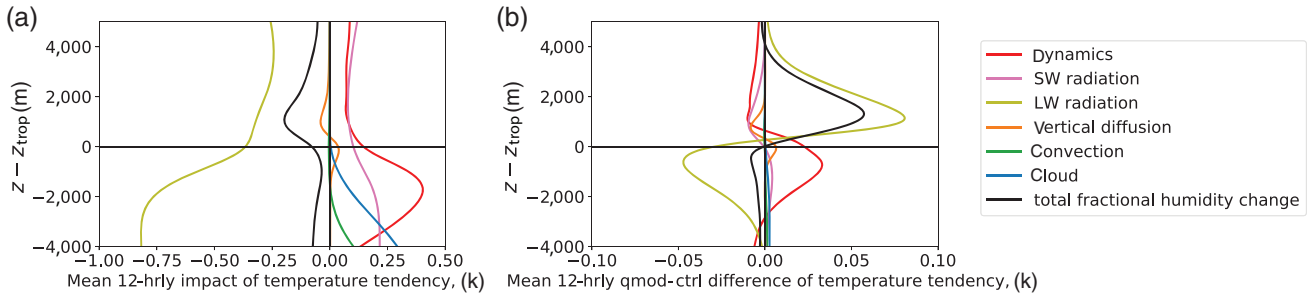

FIGURE 7 Tropopause-relative mean of (a) the Eulerian mean temperature tendencies in a 12 hr period for CTRL and (b) the QMOD minus CTRL difference between these tendencies, where a mean is taken over consecutive 12 hr periods between 24 and 120 hr into the forecast, for model resolution TCo399. [Colour figure can be viewed at wileyonlinelibrary.com]

a similar pattern, and latent heating from the cloud and convection schemes below the tropopause. The model dynamics has a mean warming effect at all tropopause-relative altitudes. Only in the troposphere are increments to temperature by cloud and convection parametrisations of comparable magnitude to radiation, dynamics, and vertical diffusion, and the mean impact of gravity wave drag is so small as to not be visible in this figure.

A conclusion drawn from Figures 4 and 5 is that the lowermost-stratospheric cold bias develops more slowly in QMOD than CTRL forecasts. This is also evident from Figure 7b, with the total mean QMOD minus CTRL difference in 12-hourly temperature tendencies above the tropopause being positive. It is also evident that this difference is primarily due to a reduction of long-wave cooling for QMOD in the lowermost stratosphere, which is expected as a result of the reduction of water vapour in this region. As discussed in the previous section, also expected from the removal of the moist bias from the lowermost stratosphere (and shown in Figure 7b) is an increase in long-wave cooling below the tropopause in QMOD. Despite this expected increase in long-wave cooling, there is only a small increase in total upper tropospheric cooling in QMOD compared with CTRL because this cooling is balanced by additional warming from the model dynamics. This additional upper tropospheric dynamical warming in QMOD appears (through comparison with Figure 7a) to be a slight amplification of the dynamic warming balancing the long-wave cooling in the upper troposphere in CTRL, before latent heating takes on a more dominant role lower down. Differences in convection and cloud between QMOD and CTRL are negligible in comparison with those in long-wave radiation. The difference in vertical diffusion temperature tendencies acts to smooth out the temperature dipole introduced by the differences in radiation, as one would expect, and is also of a much smaller magnitude than the difference in the long-wave radiation tendencies.

5.2 | Processes controlling humidity

In the CTRL forecasts, the mean UTLS humidity is approximately in an equilibrium state. This can be seen from Figure 2a, which shows that there is only a small time variation in the CTRL simulation mean vertical humidity profile, with a slight moistening in the lowermost stratosphere (which we will address later). The breakdown of mean 12-hourly increments to specific humidity from the different partitioned processes in Figure 8a shows that the specific humidity is in an approximate equilibrium state between the cloud processes, dynamics, and vertical diffusion in the UTLS. However, Figure 8c (the same as Figure 8a but with a narrower x-axis range) shows there remains a small residual in the total humidity tendency with a moistening just above the tropopause and a small drying above and below this.

In the QMOD forecasts, we unbalance this equilibrium with the initial removal of the moist bias in the lowermost stratosphere analysis. To see the impact of this removal we consider the differences in the 12-hourly development of the humidity field between QMOD and CTRL as shown in Figure 8b. The QMOD minus CTRL difference in the mean Eulerian fractional change in humidity over 12 hr, which is bringing the QMOD humidity field back towards that of the CTRL, is bimodal. The dried layer is being eroded from both the top and bottom over the course of the forecast, as can be seen by the total fractional humidity change (black line).

At the top of the dried region in QMOD, around 2–3 km above the tropopause, the additional relative moistening can be attributed to the dynamics. It can be seen in Figure 8c that in the CTRL this region is dominated by

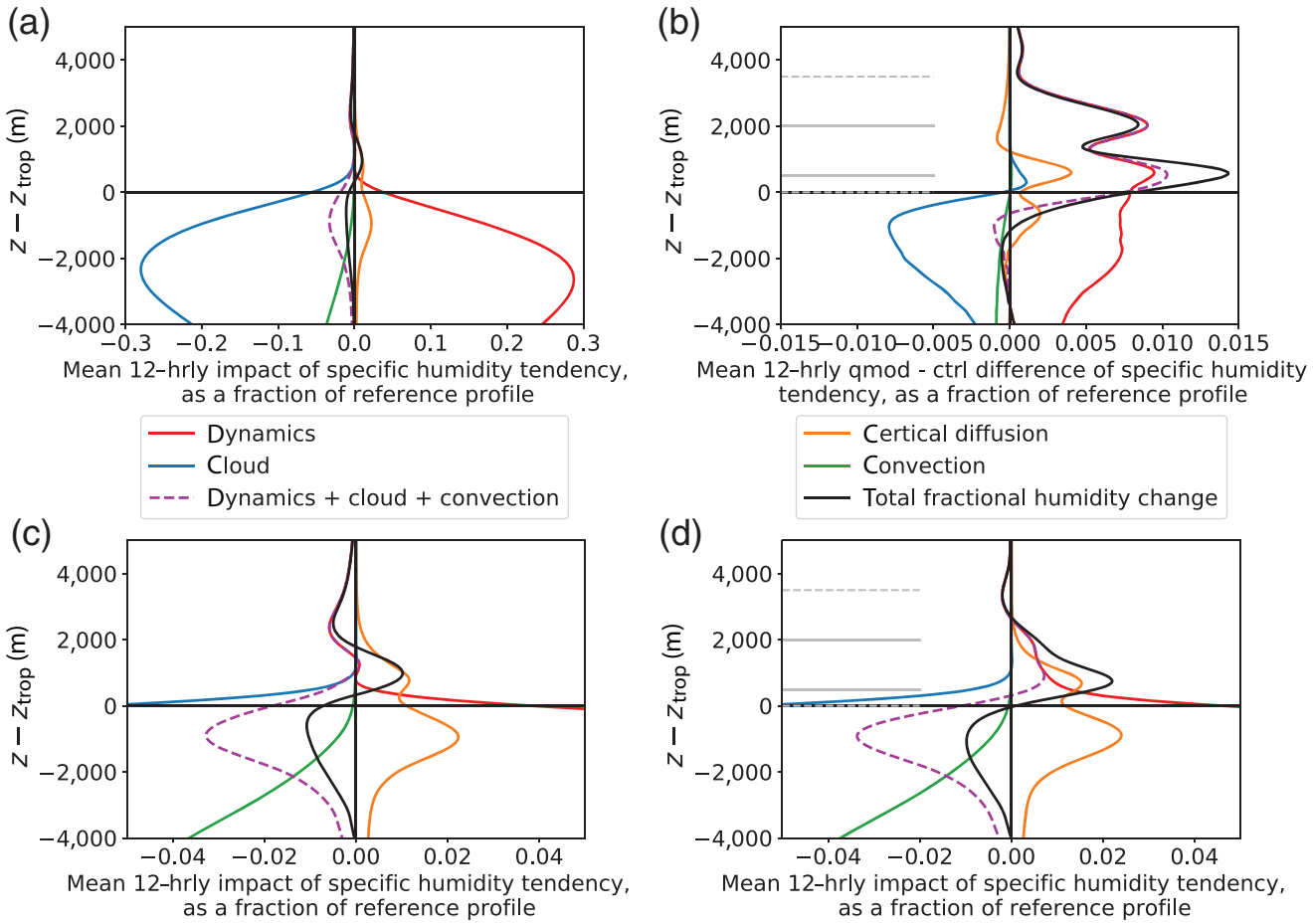

FIGURE 8 (a) Mean CTRL specific humidity tendencies and (b) the QMOD minus CTRL difference between these tendencies, as for Figure 7a,b, where here the tendencies are as a fraction of the local humidity profile. (c) The same lines as (a), but with a narrower *x*-axis. (d) The same as (c) but using data from QMOD rather than CTRL. Grey horizontal lines are as in Figure 1 to indicate the region in which the humidity was modified in QMOD. [Colour figure can be viewed at wileyonlinelibrary.com]

drying from the dynamics. However, for QMOD in Figure 8d, as we have dried this region, this is no longer the case. We hypothesise that the drying in CTRL is due to the mean descent of air in the extratropics understood within the framework of the Brewer–Dobson circulation and the mean reduction of specific humidity with altitude. In this case, for QMOD the subsidence within the lower stratosphere no longer results in drying and around 2 km above the tropopause this leads to a moistening.

At the bottom of the dried region in QMOD, with a peak at around 500 m above the tropopause, Figure 8b shows that the additional relative moistening in QMOD can be attributed to a combination of vertical diffusion and the dynamics. This moistening from the dynamics is likely to be local transport of moisture across the sharp gradient around the tropopause, with some contribution from the model dynamical core being due to numerical mixing. The CTRL in Figure 8c also shows a tendency for the model to moisten the lowermost stratosphere through vertical diffusion. Notably, in this tropopause-relative altitude framework there is no apparent sink locally balancing this source of moisture from vertical diffusion in the lowermost stratosphere, and it can be seen in Figure 2c that CTRL becomes moister than the analysis over time in the lowermost stratosphere. However, for QMOD the peak in the moistening rate in the lowest 2 km above the tropopause is more than double that of CTRL.

An additional large difference between CTRL and QMOD shown by Figure 8b is in the change to humidity by cloud processes (ice deposition) and the model dynamics in the upper troposphere. As in Figure 8a, the terms continue to cancel, but there is more drying due to cloud formation in the upper troposphere in the QMOD forecasts than in the CTRL forecasts. The upper troposphere is cooler in QMOD than CTRL, and hence has a lower saturation vapour pressure, which is a likely reason for the increased formation of upper tropospheric ice cloud. This increased removal of water vapour to cloud

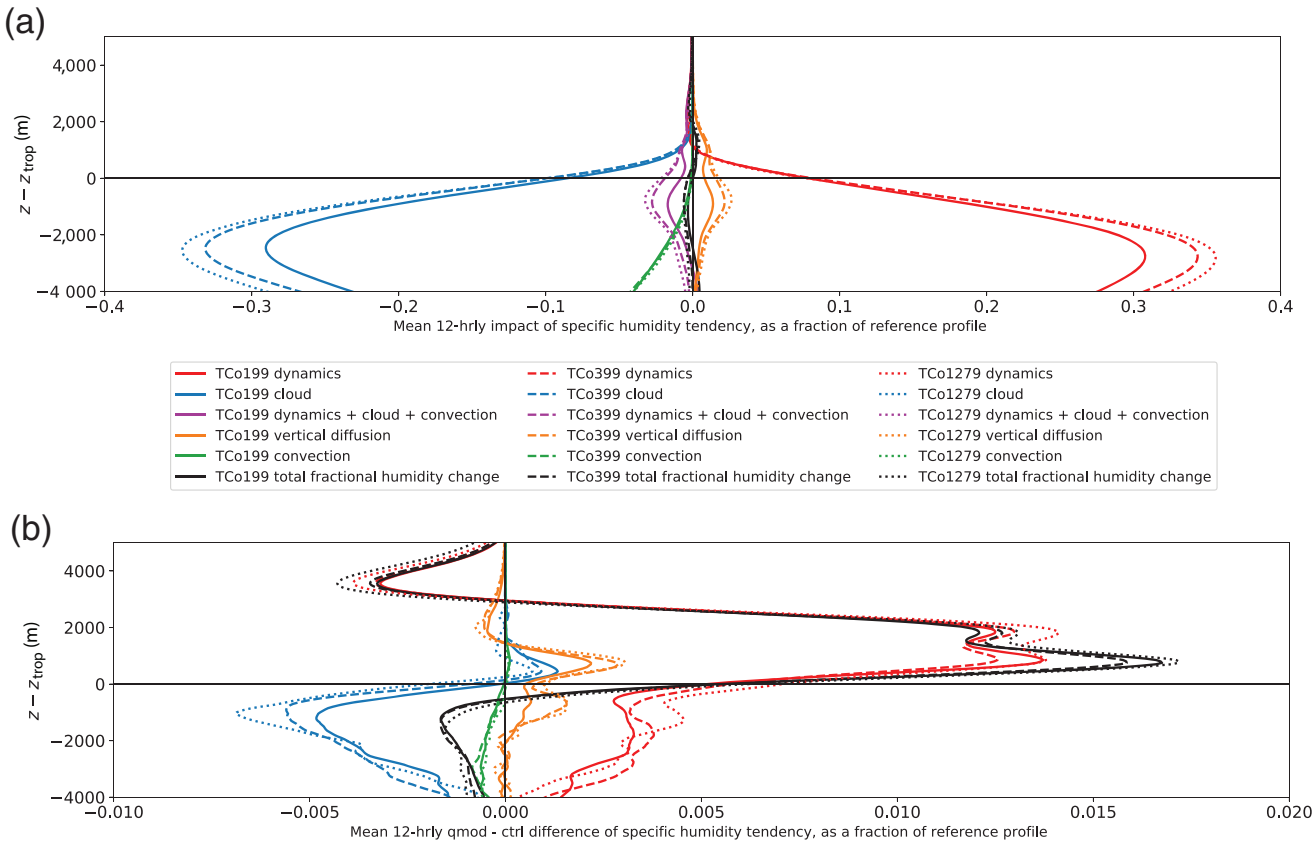

FIGURE 9 (a) Mean CTRL specific humidity tendencies and (b) the QMOD minus CTRL tendency difference (as for Figure 8a,b) for horizontal resolutions TCo199 (solid lines), TCo399 (dashed lines), and TCo1279 (dotted lines). The difference is between humidity tendencies at 48 hr and 24 hr into the forecast, and halved such that the scale is comparable to the 12-hourly differences in Figure 8; this rescaling is required because the data are only available daily for the highest resolution forecast. Note that the aspect ratio of this figure is different to that of previous figures to make the (small) differences visible. [Colour figure can be viewed at wileyonlinelibrary.com]

is balanced by an increased moistening by the model dynamics.

As well as being associated with a minimum in temperature and a sharp change in static stability, in the vicinity of the tropopause there is also a sharp change in the vertical gradient of specific humidity, accompanied by a local humidity minimum called the hygropause (which we further amplify when initialising the QMOD forecasts). The net moistening of the lowermost stratosphere we see for CTRL in Figure 8c is accompanied by a slight drying above, and a larger drying below. Necessarily (as the gradient of the sum of two fields is equivalent to the sum of the gradients), the humidity gradient across the tropopause is reduced between the local maxima of drying below and moistening above. Additionally, moistening in the lowermost stratosphere and drying above lead to an increase in the altitude of the humidity minimum. This is consistent with the result from B21 for temperature, that over the course of 5-day forecasts the tropopause is smoothed and the altitude of the tropopause systematically increases. When we artificially sharpen this moisture gradient in QMOD it is smoothed even faster by the model over the course of the forecast. That the CTRL forecasts moisten in the lowermost stratosphere can also be seen earlier from Figure 2, compared with the analysis.

It is important to note that this smoothing of the humidity field is a very local effect. The use of Eulerian tendencies in the vicinity of the tropopause, which is a very dynamic surface, means that when using a different vertical coordinate (one that is not tropopause relative), or using much longer time-scales, the signal of vertical diffusion moistening the lowermost stratosphere is not as apparent (not shown). This lack of signal is because the tendency for moistening is smoothed in the vertical with the mean drying above and particularly below; remembering that humidity decreases logarithmically with altitude and that Figure 8 shows tendencies as a fraction of the background humidity field, the local signal of drying in the upper troposphere is an order of magnitude larger than the local moistening above.

6 | EFFECTS OF HORIZONTAL RESOLUTION ON HUMIDITY BALANCE

The conclusion from Figure 2 is that there is little sensitivity of the cross-tropopause humidity transport to resolution across the three resolutions considered in this study; that is, TCo199, TCo399, and TCo1279. Here, we look at the separate humidity tendencies to see if there is any impact of resolution on the balance of the dynamical and physical processes.

It is shown by Figure 9a that the magnitudes of the cloud processes, advection of water vapour by dynamics, vertical diffusion, and the net reduction of humidity in the upper troposphere by the difference between dynamics and cloud all increase with increasing horizontal resolution. However, the resolution dependence of the total mean change to the humidity profile is nearly zero because the process tendency changes cancel each other out.

Figure 2 showed that the TCo1279 QMOD forecast remoistened towards the analysis slightly faster than in the lower resolution forecasts. Figure 9b illustrates that this difference is due to both an increase in the relative remoistening at the top of the dried layer by changes to the effects of subsidence and by increased vertical diffusion from below across the tropopause. This difference is despite the vertical level spacing being the same across all three horizontal resolutions.

7 | DISCUSSION AND CONCLUSIONS

Previous studies have shown that the reason for a significant cold bias in the extratropical lowermost stratosphere in many global weather forecast and climate models, including the IFS, is at least in part due to an overestimate of the amount of water vapour in the lowest few kilometres above the tropopause, leading to excessive long-wave radiative cooling. The overall aim of this study is to gain a deeper understanding of the characteristics of this moist bias and its impact on the cooling, in both the initial conditions and through the forecast, and to attribute the causes of the moist bias to model processes and resolution.

Sets of 30 5-day and 15-day forecast simulations with the IFS are performed for three different horizontal resolutions initialised daily at 0000 UTC for the 15 September to 14 October 2016. This period was chosen to coincide with the NAWDEX field campaign (Schäfler *et al.*, 2018), from which radiosonde observations were used by Bland *et al.* (2021) to characterise the UTLS temperature and humidity biases. Given that the moist bias is apparent in the operational analyses used for initialising the forecasts, one set of forecasts is performed with the mean moist bias removed from the extratropical lowermost stratosphere in the initial analyses (QMOD) based on observational humidity data from radiosondes (Bland *et al.*, 2021) and the MLS, and the second set is unmodified and provides the control forecasts (CTRL) for comparison.

As there are very few humidity measurements used to constrain the analysis state above the tropopause, the humidity in the lowermost stratosphere will be dependent on the model dynamics and parametrised physical processes, and any biases in these processes will lead to a biased quasi-equilibrium in the analysis that persists into the forecast. The QMOD "corrected" humidity analyses have, on average, around 40% of the water vapour removed in the lowermost stratosphere to bring them closer to the observed humidity.

First, the impact of reducing the humidity bias in the analysis on the temperature and humidity evolution through the forecast is determined by comparing QMOD and CTRL. Following the more realistic reduction of humidity from the lowermost stratosphere in the initial conditions in QMOD, the development of the cold bias in the lowermost stratosphere is significantly reduced, with the cold bias growth rate approximately halved in QMOD compared with CTRL. Associated with the reduced temperature change, the systematic bias of the tropopause being at too high an altitude in CTRL is reduced also for QMOD. Regarding the humidity evolution from the drier corrected initial state, the modified region starts to remoisten towards the "equilibrium" values in CTRL with a half-life of 8–9 days. The fact that the cold bias still grows through the forecast in QMOD, albeit at a reduced rate, could be due to this gradual remoistening. However, it is likely to be a small effect initially, and other experiments in which the humidity reduction is applied through the forecast to the water vapour seen by the radiation show a similar cooling (not shown), which suggests the remoistening is not the main cause of the remaining cold bias growth. Other reasons could be the imperfect methodology to remove the humidity bias, which is an average correction, or from other local sources of cooling, such as gravity wave breaking or gas radiative properties, not investigated here; experiments elsewhere have shown that uncertainty in the gas optics representation for the radiation parametrisation can also lead to temperature changes in the extratropical lowermost stratosphere (R. Hogan, personal communication).

Addressing the attribution question, the reduction in the cooling in the lowermost stratosphere is confirmed here to be almost entirely a result of a reduction in long-wave radiation when the lowermost stratosphere has reduced water vapour. There is little concurrent increase in cooling in the upper troposphere in QMOD, as a dipole of cooling below warming would be expected from a localised

reduction in humidity—as seen in the single column model experiments in B21. This is because the increase in below-tropopause radiative cooling is largely balanced by the model dynamics. Moisture is reintroduced at both the top and bottom of the dried layer in QMOD by the model dynamics, and additionally at the bottom by the subgrid turbulent mixing parametrisation (vertical diffusion). In the CTRL forecasts in a tropopause-relative frame of reference, vertical diffusion acts to moisten the lowest kilometre of the stratosphere, and there is no sink of moisture to balance this. The role of cloud microphysics (as a sink of water vapour through ice deposition) does not change significantly above the tropopause when the humidity is reduced, which suggests that local cloud processes have little control on the moist bias in the extratropical lowermost stratosphere. The result that the bias seems to be largely controlled by subgrid vertical diffusion and the dynamics is consistent with the conclusions of Krüger *et al.* (2022) that the moist bias is likely to be a result of the model representation of mixing across the tropopause.

The partial attribution of the remoistening to the dynamical advection of water vapour could either be as a result of a moist bias in the source region (above and/or below), a misrepresentation of, or an overdiffusive, resolved transport, or excessive implicit diffusion from the dynamics. Owing to the short time-scales of the moist bias reintroduction, and the isolation of the bias to the lowest 2 km of the extratropical stratosphere, the key processes are most likely to be upwards mixing from the extratropical upper troposphere or quasi-isentropic transport from the subtropical upper troposphere. A further conclusion from this study is that changes to horizontal resolution of the IFS from TCo199 (50 km grid spacing) to TCo1279 (9 km grid spacing) make very little difference to the overall rate of moistening of the lowermost stratosphere. This suggests the moist bias cannot be attributed to insufficiently resolved horizontal motion. However, the isentropic transport from the subtropical upper troposphere into the extratropical lowermost stratosphere is observed to occur often in thin layers, so vertical resolution may play a role. A consequence of too low a vertical resolution in the model will be to mix the higher humidity from these layers too rapidly. It is possible that there would be more of an impact at horizontal and vertical resolutions lower than are used here. Stenke *et al.* (2008) found a moist/cold lowermost stratosphere bias in the ECHAM4 model using a semi-Lagrangian advection scheme, which was significantly reduced when using a Lagrangian advection scheme with much reduced horizontal mixing across the tropopause. However, this difference may be due to the much lower spectral resolution (T30) and lower vertical resolution (39 levels) used in their simulations. These results are also consistent with findings by Hardiman *et al.* (2015), that biases in tropical near-tropopause temperature and humidity can be reduced through improvements to the interpolation used for the vertical advection, and Charlesworth *et al.* (2023), that when using fully Lagrangian transport for water vapour above 250 hPa the moist bias is greatly reduced.

There are several limitations of this study that should be noted. First, the humidity correction is applied as a relatively simple formula to give agreement with the radiosonde and MLS observations in an average sense, as the detailed structure of the error is not known. This may not be optimal but was determined to be the best approximation in the absence of extensive observations to define the spatial structure of the error in the analysis at each time. Second, the forecast period only covers a month in the boreal autumn of a single year, and results are shown only for the Northern Hemisphere extratropics. Some ways in which our considered period deviated from the climatological average include that there was more warm conveyor belt activity over the North Atlantic, and that there was persistent high pressure over Scandinavia in October (Schäfler *et al.*, 2018). Other studies suggest the cold bias is larger in the summer hemisphere and smaller in the winter hemisphere (e.g., Dyroff *et al.* (2015)), so an extension of the evaluation to other seasons and to cover the Southern Hemisphere as well would be beneficial; but again, this is limited by a lack of observations to fully characterise the humidity bias. Third, only the ECMWF IFS global weather forecast model is investigated here and it would be interesting to apply the same evaluation to other weather and climate models in the future to assess the wider applicability of the results.

There are, however, several overall conclusions from this study for the IFS that are likely to be generally applicable to other models: (a) in order to reduce the cold temperature bias in the extratropical lowermost stratosphere, any moist bias in this region must be reduced; (b) improvements may be required to the advection of water vapour and subgrid turbulent mixing in the region of the tropopause. Clearly, at least for the IFS, improvements to the model dynamics and physics will be required to significantly reduce the moist and cold bias in the extratropical lowermost stratosphere. While improving the use and availability of water vapour observations in the lowermost stratosphere in the assimilation schemes used for operational analyses and reanalyses should be explored to help constrain the humidity in this region, owing to the remoistening effects from the model, improvements to the humidity in the initial conditions are alone insufficient to correct the cold bias in the medium to long range.

Further directions for study should include a systematic assessment of the role of vertical resolution and the sensitivity to changes to the dynamics advection and

turbulent mixing parametrisation to reduce the excessive transport/mixing of water vapour into the lowermost stratosphere. An understanding of other possible sources of a temperature bias in this region, such as the radiative properties of atmospheric gases, is also required. In addition to water vapour, ozone is another radiatively important trace gas in the lowermost stratosphere, as shown by Randel *et al.* (2007). Finally, the next step is an assessment of the meteorological impacts that correcting the cold bias in the extratropical lowermost stratosphere would have on the upper level jets (by reducing the bias in the meridional temperature gradient), and thereby the representation of Rossby waves and predictive skill across forecast lead times.

ACKNOWLEDGEMENTS

Jake Bland was funded by the Natural Environment Research Council (NERC) SCENARIO Doctoral Training Partnership (NE/L002566/1). With thanks to three anonymous reviewers for their useful comments.

CONFLICT OF INTEREST STATEMENT

The authors state there are no competing interests.

DATA AVAILABILITY STATEMENT

The IFS forecast data for the simulations used in this study are available from ECMWF upon request from the corresponding author.

The data that support the findings of this study are available on MARS. DOIs for these have not yet been issued, but will be at a later date.

ORCID

Jake Bland https://orcid.org/0000-0003-2706-2853
Richard Forbes https://orcid.org/0000-0002-3596-8287
Suzanne L. Gray https://orcid.org/0000-0001-8658-362X
John Methven https://orcid.org/0000-0002-7636-6872

REFERENCES

Bland, J., Gray, S., Methven, J. & Forbes, R. (2021) Characterising extratropical near-tropopause analysis humidity biases and their radiative effects on temperature forecasts. *Quarterly Journal of the Royal Meteorological Society*, 147(741), 3878–3898. Available from: https://doi.org/10.1002/QJ.4150

Boljka, L. & Birner, T. (2022) Potential impact of tropopause sharpness on the structure and strength of the general circulation. *Nature Partner Journals Climate and Atmospheric Science*, 5(1), 1–9. Available from: https://doi.org/10.1038/s41612-022-00319-6

Bönisch, H., Engel, A., Curtius, J., Birner, T. & Hoor, P. (2009) Quantifying transport into the lowermost stratosphere using simultaneous in-situ measurements of SF6 and CO2. *Atmospheric Chemistry and Physics*, 9(16), 5905–5919. Available from: https://doi.org/10.5194/acp-9-5905-2009

Bradshaw, N.G., Vaughan, G., Busen, R., Garcelon, S., Jones, R., Gardiner, T. et al. (2002) Tracer filamentation generated by small-scale Rossby wave breaking in the lower stratosphere. *Journal of Geophysical Research: Atmospheres*, 107(D23), ACL 12–1. Available from: https://doi.org/10.1029/2002JD002086

Cau, P., Methven, J. & Hoskins, B. (2005) Representation of dry tropical layers and their origins in ERA-40 data. *Journal of Geophysical Research: Atmospheres*, 110(D6), 1–11. Available from: https://doi.org/10.1029/2004JD004928

Charlesworth, E., Plöger, F., Birner, T., Baikhadzhaev, R., Abalos, M., Abraham, N.L. et al. (2023) Stratospheric water vapor affecting atmospheric circulation. *Nature Communications*, 14, 3925. Available from: https://doi.org/10.1038/s41467-023-39559-2

Dyroff, C., Zahn, A., Christner, E., Forbes, R., Tompkins, A.M. & van Velthoven, P.F.J. (2015) Comparison of ECMWF analysis and forecast humidity data with CARIBIC upper troposphere and lower stratosphere observations. *Quarterly Journal of the Royal Meteorological Society*, 141(688), 833–844. Available from: https://doi.org/10.1002/qj.2400

ECMWF. (2020) IFS documentation CY47R1 - part IV: physical processes — ECMWF. In: *IFS documentation CY47R1*. Reading: ECMWF. Available from: https://www.ecmwf.int/en/elibrary/81189-ifs-documentation-cy47r1-part-iv-physical-processes

Gettelman, A., Hegglin, M.I., Son, S.-W., Kim, J., Fujiwara, M., Birner, T. et al. (2010) Multimodel assessment of the upper troposphere and lower stratosphere: tropics and global trends. *Journal of Geophysical Research*, 115(D3), D00M08. Available from: https://doi.org/10.1029/2009JD013638

Hardiman, S.C., Boutle, I.A., Bushell, A.C., Butchart, N., Cullen, M.J.P., Field, P.R. et al. (2015) Processes controlling tropical tropopause temperature and stratospheric water vapor in climate models. *Journal of Climate*, 28(16), 6516–6535. Available from: https://doi.org/10.1175/JCLI-D-15-0075.1

Ingleby, B. (2017) An assessment of different radiosonde types 2015/2016 — ECMWF. *ECMWF Technical Memoranda*, 807(80268), 1–69. Available from: https://www.ecmwf.int/en/elibrary/17551-assessment-different-radiosonde-types-2015-2016 [Accessed 12th November 2018].

Jensen, E.J., Pan, L.L., Honomichl, S., Diskin, G.S., Krämer, M., Spelten, N. et al. (2020) Assessment of observational evidence for direct convective hydration of the lower stratosphere. *Journal of Geophysical Research: Atmospheres*, 125(15), e2020JD032793. Available from: https://doi.org/10.1029/2020JD032793

Joshi, M.M., Charlton, A.J. & Scaife, A.A. (2006) On the influence of stratospheric water vapor changes on the tropospheric circulation. *Geophysical Research Letters*, 33(9), L09806. Available from: https://doi.org/10.1029/2006GL025983

Krüger, K., Schäfler, A., Wirth, M., Weissmann, M. & Craig, G.C. (2022) Vertical structure of the lower-stratospheric moist bias in the ERA5 reanalysis and its connection to mixing processes. *Atmospheric Chemistry and Physics*, 22(23), 15559–15577. Available from: https://doi.org/10.5194/ACP-22-15559-2022

Kunkel, D., Hoor, P., Kaluza, T., Ungermann, J., Kluschat, B., Giez, A. et al. (2019) Evidence of small-scale quasi-isentropic mixing in ridges of extratropical baroclinic waves. *Atmospheric Chemistry and Physics*, 19(19), 12607–12630. Available from: https://doi.org/10.5194/ACP-19-12607-2019

Kunz, A., Spelten, N., Konopka, P., Müller, R., Forbes, R.M. & Wernli, H. (2014) Comparison of fast in situ stratospheric hygrometer (FISH) measurements of water vapor in the upper troposphere and lower stratosphere (UTLS) with ECMWF (re)analysis data. *Atmospheric Chemistry and Physics*, 14, 10803–10822. Available from: https://doi.org/10.5194/acp-14-10803-2014

Lambert, A., Read, W., Livesey, N. & Fuller, R. (2020) MLS/Aura Level 3 Daily Binned Water Vapor (H2O) Mixing Ratio on Assorted Grids V004. https://doi.org/10.5067/Aura/MLS/DATA/3109

Lawrence, Z.D., Abalos, M., Ayarzagüena, B., Barriopedro, D., Butler, A.H., Calvo, N. et al. (2022) Quantifying stratospheric biases and identifying their potential sources in subseasonal forecast systems. *Weather and Climate Dynamics Discussions*, 2022, 1–37. Available from: https://doi.org/10.5194/wcd-3-977-2022

Livesey, N.J., Read, W.G., Wagner, P.A., Froidevaux, L., Lambert, A., Manney, G.L. et al. (2020) Version 4.2x Level 2 and 3 data quality and description document. https://mls.jpl.nasa.gov/data/v4-2

Malardel, S., Wedi, N., Deconinck, W., Diamantakis, M., Kühnlein, C., Mozdzynski, G. et al. (2016) A new grid for the IFS. *ECMWF Newsletter*, 146(80059), 23–28. Available from: https://doi.org/10.21957/zwdu9u5i

Maycock, A.C., Joshi, M.M., Shine, K.P. & Scaife, A.A. (2013) The circulation response to idealized changes in stratospheric water vapor. *Journal of Climate*, 26(2), 545–561. Available from: https://doi.org/10.1175/JCLI-D-12-00155.1

Müller, S., Hoor, P., Berkes, F., Bozem, H., Klingebiel, M., Reutter, P. et al. (2015) In situ detection of stratosphere-troposphere exchange of cirrus particles in the midlatitudes. *Geophysical Research Letters*, 42(3), 949–955. Available from: https://doi.org/10.1002/2014GL062556

Noël, S., Weigel, K., Bramstedt, K., Rozanov, A., Weber, M., Bovensmann, H. et al. (2018) Water vapour and methane coupling in the stratosphere observed using SCIAMACHY solar occultation measurements. *Atmospheric Chemistry and Physics*, 18(7), 4463–4476. Available from: https://doi.org/10.5194/ACP-18-4463-2018

O'Connor, F.M., Vaughan, G. & Backer, H.D. (1999) Observations of subtropical air in the european mid-latitude lower stratosphere. *Quarterly Journal of the Royal Meteorological Society*, 125(560), 2965–2986. Available from: https://doi.org/10.1002/QJ.49712556009

Oikonomou, E.K. & O'Neill, A. (2006) Evaluation of ozone and water vapor fields from the ECMWF reanalysis ERA-40 during 1991–1999 in comparison with UARS satellite and MOZAIC aircraft observations. *Journal of Geophysical Research*, 111(D14), D14109. Available from: https://doi.org/10.1029/2004JD005341

Polichtchouk, I., Bechtold, P., Diamantakis, M., Forbes, R., Hogan, R., Malardel, S. et al. (2019a) Causes and fixes for stratospheric temperature biases in IFS and their impact on predictability. *Workshop on Stratospheric Predictability and Impact on the Troposphere*. Reading, 18–21 November. Available from: https://events.ecmwf.int/event/129/contributions/1110/attachments/286/526/Stratospheric-WS-Polichtchouk.pdf [Accessed 9th February 2024].

Polichtchouk, I., Diamantakis, M. & Vana, F. (2020) *Quintic vertical interpolation improves forecasts of the stratosphere*. Reading: ECMWF. Available from: https://doi.org/10.21957/ip52yu935j

Polichtchouk, I., Stockdale, T., Bechtold, P., Diamantakis, M., Malardel, S., Sandu, I. et al. (2019b) Control on stratospheric temperature in IFS: resolution and vertical advection. *ECMWF Technical Memoranda*, 847(81078), 1–36. Available from: https://doi.org/10.21957/cz3t12t7e

Randel, W.J., Wu, F. & Forster, P. (2007) The extratropical tropopause inversion layer: global observations with GPS data, and a radiative forcing mechanism. *Journal of the Atmospheric Sciences*, 64(12), 4489–4496. Available from: https://doi.org/10.1175/2007JAS2412.1

Rodwell, M.J. & Palmer, T.N. (2007) Using numerical weather prediction to assess climate models. *Quarterly Journal of the Royal Meteorological Society*, 133(622), 129–146. Available from: https://doi.org/10.1002/QJ.23

Schäfler, A., Craig, G., Wernli, H., Arbogast, P., Doyle, J.D., McTaggart-Cowan, R. et al. (2018) The North Atlantic waveguide and downstream impact experiment. *Bulletin of the American Meteorological Society*, BAMS–D–17–0003.1, 99(8), 1607–1637. Available from: https://doi.org/10.1175/BAMS-D-17-0003.1

Shepherd, T.G., Polichtchouk, I., Hogan, R.J. & Simmons, A.J. (2018) Report on stratosphere task force. *ECMWF Technical Memoranda*, 824(18259), 32.

Stenke, A., Grewe, V. & Ponater, M. (2008) Lagrangian transport of water vapor and cloud water in the ECHAM4 GCM and its impact on the cold bias. *Climate Dynamics*, 31(5), 491–506. Available from: https://doi.org/10.1007/s00382-007-0347-5

Tandon, N.F., Polvani, L.M. & Davis, S.M. (2011) The response of the tropospheric circulation to water vapor-like forcings in the stratosphere. *Journal of Climate*, 24(21), 5713–5720. Available from: https://doi.org/10.1175/JCLI-D-11-00069.1

Vaisala. (2013) Vaisala Radiosonde RS92-SGP. Technical report https://www.bodc.ac.uk/data/documents/nodb/pdf/RS92SGP-Datasheet-B210358EN-F

Vaisala. (2018) Radiosonde RS41-SG. Technical report https://docs.vaisala.com/v/u/B211321EN-K/en-US [Accessed 4th September 2019].

Vaughan, B.G. & Timmis, C. (1998) Transport of near-tropopause air into the lower midlatitude stratosphere. *Quarterly Journal of the Royal Meteorological Society*, 124(549), 1559–1578. Available from: https://doi.org/10.1002/QJ.49712454910

Woiwode, W., Dörnbrack, A., Polichtchouk, I., Johansson, S., Harvey, B., Höpfner, M. et al. (2020) Technical note: lowermost-stratospheric moist bias in ECMWF IFS model diagnosed from airborne GLORIA observations during winter/spring 2016. *Atmospheric Chemistry and Physics*, 20(23), 15379–15387. Available from: https://doi.org/10.5194/acp-2020-367

Wu, Z. & Reichler, T. (2020) Variations in the frequency of stratospheric sudden warmings in CMIP5 and CMIP6 and possible causes. *Journal of Climate*, 33(23), 10305–10320. Available from: https://doi.org/10.1175/JCLI-D-20-0104.1

How to cite this article: Bland, J., Forbes, R., Gray, S.L. & Methven, J. (2024) Processes controlling extratropical near-tropopause humidity and temperature in the ECMWF global weather forecast model. *Quarterly Journal of the Royal Meteorological Society*, 1–17. Available from: https://doi.org/10.1002/qj.4873